JACS
JOURNAL OF THE AMERICAN CHEMICAL SOCIETY
pubs.acs.org/JACS
Article

Real-Space Imaging of a Single-Molecule Monoradical Reaction

Shaotang Song,[#] Na Guo,[#] Xinzhe Li, Guangwu Li, Yohei Haketa, Mykola Telychko, Jie Su, Pin Lyu, Zhizhan Qiu, Hanyan Fang, Xinnan Peng, Jing Li, Xinbang Wu, Ying Li, Chenliang Su, Ming Joo Koh, Jishan Wu, Hiromitsu Maeda, Chun Zhang, and Jiong Lu*

Cite This: J. Am. Chem. Soc. 2020, 142, 13550−13557
Read Online

ACCESS | Metrics & More | Article Recommendations | Supporting Information

ABSTRACT: Organic radicals consisting of light elements exhibit a low spin−orbit coupling and weak hyperfine interactions with a long spin coherence length, which are crucial for future applications in molecular spintronics. However, the synthesis and characterization of these organic radicals have been a formidable challenge due to their chemical instability arising from unpaired electrons. Here, we report a direct imaging of the surface chemical transformation of an organic monoradical synthesized via the monodehydrogenation of a chemically designed precursor. Bond-resolved scanning tunneling microscopy unambiguously resolves various products formed through a complex structural dissociation and rearrangement of organic monoradicals. Density functional theory calculations reveal detailed reaction pathways from the monoradical to different cyclized products. Our study provides unprecedented insights into complex surface reaction mechanisms of organic radical reactions at the single molecule level, which may guide the design of stable organic radicals for future quantum technology applications.

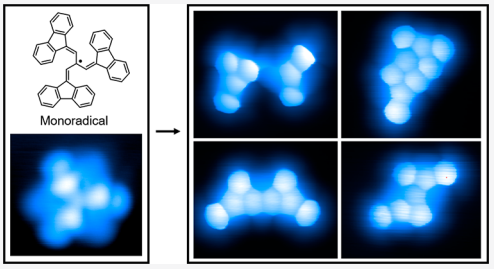

INTRODUCTION

The first isolation of organic radicals dates back to 1900, when Gomberg obtained triphenylmethyl in carbon dioxide atmosphere.[1] Since then, organic radicals have long fascinated chemists because they are not only fundamentally interesting but also possess numerous potential applications in diverse fields including organic magnetism, MRI contrast agents, and spintronics.[2−5] In particular, these molecules consisting of light elements have low spin−orbit coupling and weak hyperfine interactions, leading to a longer spin coherence length than that of heavy transition metal-based magnetic compounds.[6] Because of these figure-of-merits, organic radicals show a great promise in molecular spintronics, where long spin coherence length is required to preserve the information encoded in the electron spin.[3] However, the direct synthesis and characterization of organic radicals with large and tunable net spin has been a long-standing challenge due to their high chemical instability arising from the presence of unpaired electrons.[7]

Common strategies involving kinetic protections and thermodynamic stabilizations have been widely used to enhance the stability of the radicals. Despite recent encouraging progress, the facile synthesis of stable organic radicals under ambient condition still remains elusive.[7] The intrinsic high reactivity of these materials often leads to the formation of numerous byproducts through undesired structural dissociation, dimerization, and oxidation reactions.[8] The ability to understand the complex chemical transformation of organic radicals at the single-molecule level not only sheds light into fundamental radical chemistry but also provides new insights into the design of stable organic radicals for future applications. Unfortunately, identifying the chemical structures of reaction intermediates and byproducts derived from organic radicals using conventional characterization techniques requires the isolation of individual molecules, which is rather challenging due to the short lifetime of these radical species under ambient conditions.

Recent advance in scanning tunneling microscopy (STM) with molecule-functionalized tip, namely bond-resolved STM (BRSTM), allows for submolecular resolution imaging of the internal bond structures of individual molecules without the additional complexity of noncontact atomic force microscopy.[9−15] The constant-height BRSTM imaging was conducted in the Pauli repulsion regime using a carbon-monoxide (CO) functionalized STM tip. In this regime, the CO molecule at the tip-apex undergoes a lateral bending with the largest deflection magnitude over the electron-rich areas presented by chemical bonds.[13] Such a deflection of the CO molecule effectively modulates the overall tunnelling conductance of the tip−sample junction, leading to the appearance of sharp line features over the positions of chemical bonds in the tunnelling current image. Here, we utilized this technique to investigate the surface reaction of a monoradical at the single-molecule

Received: May 18, 2020
Published: July 7, 2020

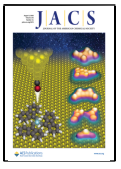

https://dx.doi.org/10.1021/jacs.0c05337
J. Am. Chem. Soc. 2020, 142, 13550−13557

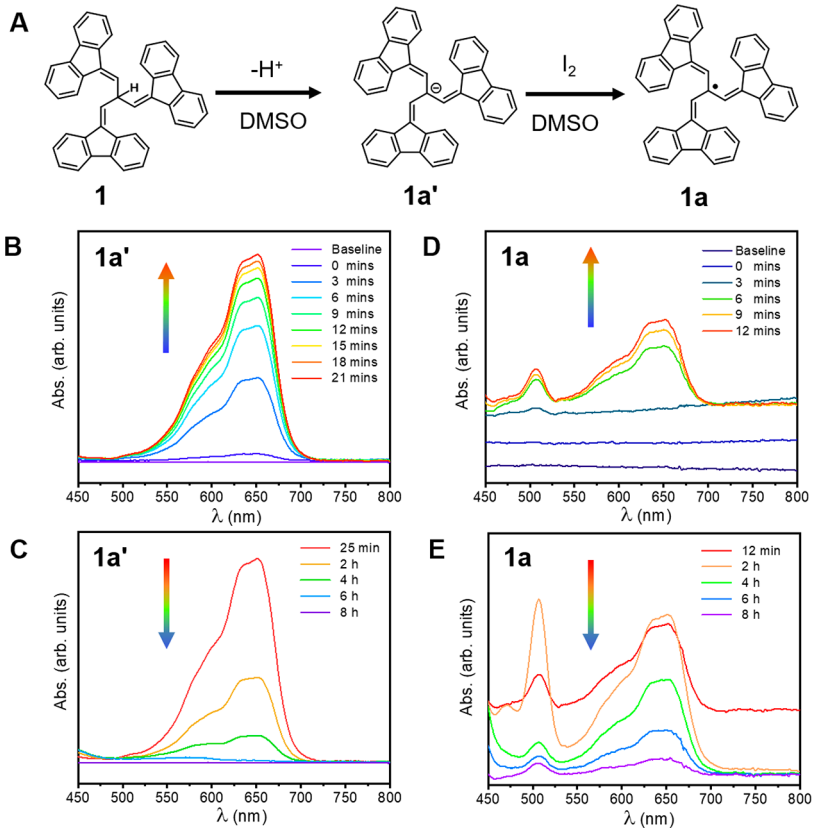

Figure 1. (A) A schematic illustration of the generation of anion **1a**′ and monoradical **1a** in DMSO. (B and C) Probe the lifetime of in-solution generated anion **1a**′ under ambient condition using UV−vis spectroscopy. The evolution of absorption features (B) before and (C) after the absorption intensity reaches its maximum. (D and E) Probe the lifetime of monoradical **1a** generated by I_2-induced oxidation of the anion. The evolution of absorption features (D) before and (E) after the peak intensity at 652 nm reaches its maximum.

level, whereby a cascade structural rearrangements into various products are directly captured.[16,17] The precursor **1** (Figure 2A) consists of three fluorene moieties on the periphery connected by an isobutane group in the center (refer to Scheme S1 for the synthetic procedure). The monoradical **1a** can be generated through the monodehydrogenation of precursor **1** during the thermal evaporation (Figure 2A) and subsequently deposited on the surface as supported by a combination of thermal gravimetric analysis (TGA) study (Figure S7) and large-scale STM imaging (Figure 2E). The removal of one hydrogen atom attached to the sp^3 hybridized carbon atom in the center generates the monoradical (**1a**), which can be stabilized by the delocalization of the unpaired electron to the adjacent fluorene moieties (Figures 2A and S2).

Surface-assisted thermal dehydrogenation can be utilized to synthesize monoradical **1a** on Au(111) substrate under ultrahigh vacuum (UHV) conditions, whereby both structural and spin properties can be characterized by STM at the single-molecule level.[14,18−21] Moreover, a gentle thermal treatment can induce the formation of various hydrocarbon on surface via intra- and intermolecular bond rearrangements, which can be directly imaged by BRSTM with submolecular resolution.[9,10,22,23] Finally, the coupling between two fluorene radicals on Au(111) produces rubicene, an important heptacyclic arene known for over a century.[24]

RESULTS AND DISCUSSION

Probe the Lifetime of Anions and Radicals Generated in Solution Phase. Prior to on-surface synthesis and characterization of monoradicals, we conducted in-solution synthesis of monoradical **1a** and monitor its transformation via UV−vis spectroscopy under ambient conditions, which can provide insights into its chemical reactivity and stability. Monoradical **1a** can be generated by iodine-induced oxidation of the corresponding anion **1a**′ in solution phase (Figure 1A). First, the solution of precursor **1** dissolved in dimethyl sulfoxide (DMSO) gradually turns to a blue color, suggesting the formation of anion **1a**′ species with UV−vis absorbance between 550 and 700 nm (Figure 1B), consistent with absorption spectrum calculated by time-dependent density functional theory (TD-DFT) (Figure S6). The maximal absorption occurs after exposing the solution for 21 min in air, attributed to a complete dehydrogenation of precursor **1** into anion **1a**′. The highest absorption band at λ = 652 nm is associated with HOMO → LUMO and HOMO → LUMO+1 transitions according to TD-DFT calculations (Figure S6). These absorption features vanish after 8 h (Figure 1C), suggesting a relatively short lifetime of the anion in air due to its high reactivity, consistent with previous report.[25] Subsequently, we performed iodine-induced oxidization of the anion to generate the monoradical **1a** in solution. New absorption features between 475 and 575 nm (Figure 1D) appear right after adding iodine into a freshly prepared solution of precursor **1**. TD-DFT calculations reveal that these absorption features are mainly contributed from the SOMO → SUMO transition (Figure S6). The peak intensity around λ = 652 nm reaches its maximum at 12 min and then starts to decrease due to the oxidation of anion to monoradical (Figure

https://dx.doi.org/10.1021/jacs.0c05337
J. Am. Chem. Soc. 2020, 142, 13550−13557

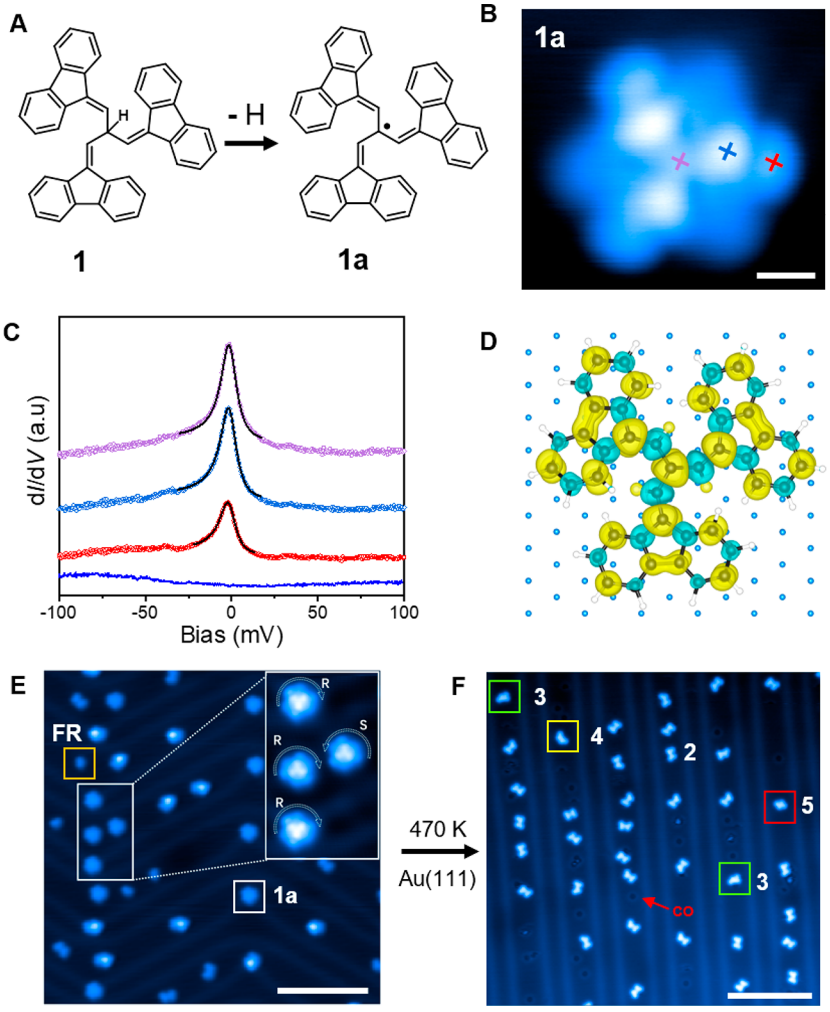

Figure 2. (A) Illustration of the formation of monoradical **1a** via monodehydrogenation of compound **1**. (B) Constant current STM image of monoradical **1a** (I = 100 pA, V = 50 mV). Scale bar in B is 0.5 nm. (C) dI/dV spectra taken at different position over molecule **1a** marked by a cross in panel B. The zero-bias peaks can be fitted with Fano function (black solid lines overlaid with the experimental data). Blue solid spectrum taken at Au(111) as reference. (D) Calculated spin density distribution of **1a** on Au(111). Yellow and green isosurfaces denote spin up and spin down populations, respectively. (E) Large-scale STM image (metallic tip, I = 100 pA, V = 1.5 V) reveals the formation of monoradical **1a** coexisting with fluorene radical and nonplanar molecular fragments after the thermal evaporation and deposition of precursor **1** onto the Au(111) substrate (inset: magnified view shows monoradical **1a** molecules with left-handed and right-handed chirality). (F) Large-scale STM image (CO tip, I = 100 pA, V = 1.5 V) of the four products (**2**, **3**, **4**, and **5**) after thermal annealing of monoradical **1a** on Au(111) at 470 K. Scale bars in E and F are 10 nm.

1E). As a result, the peak at λ = 506 nm increases in intensity within 2 h. In addition, the absorption peaks at 506, 547, and 652 nm nearly vanish after 8 h, which indicates a similar short lifetime of both anion and monoradical under ambient conditions. The short lifetime of these chemical species poses a great challenge for structural identification of a mixture of products using conventional ensemble techniques, such as nuclear magnetic resonance or mass spectroscopy.

Real-Space Imaging of on-Surface Monoradical Reaction. We deposited precursor **1** via thermal sublimation at 410 K onto Au(111) held at 300 K. Subsequent STM imaging reveals that a dominant molecular species with hexagonal geometry coexisted with several molecular fragments with different STM contrast (Figure 2E). As shown in the magnified STM image (Figure 2B), hexagonal-shaped molecules exhibit alternate bright and dim features on the periphery of the molecule, which can be assigned to the adjacent three fluorenyl motifs. We noted that the sublimation of precursor **1** only occurs above 410 K in UHV condition, higher than its decomposition temperature (383 K) obtained by TGA (Figure S7). Therefore, it is very likely that precursor **1** has transformed into monoradical **1a** or decomposed into fluorene radical (**FR**) and other nonplanar molecular fragments (Figures 2E and S4). These smaller molecular fragments with low molecular weight are likely to desorb during the subsequent thermal annealing for thermal activation of monoradical **1a** reactions. The generation of monoradical **1a** can be further supported by the prominent zero-bias peaks (ZBP) in dI/dV spectra (Figure 2C) acquired at different positions above the molecule on Au(111) (Figure 2B). The ZBP features can be well fit with a Fano function[26−28] (refer to the details in Supporting Information) and thus are attributed to Kondo resonances arising from the screening of magnetic moment (unpaired electron in monoradical **1a**) by the conduction electrons residing in the Au(111) (Figure 2C).[3,5,18,29−31] In addition, DFT calculation reveals (Figure 2D) that the spin density of **1a** is delocalized over the whole molecular backbone on Au(111), in good agreement with the

https://dx.doi.org/10.1021/jacs.0c05337
J. Am. Chem. Soc. 2020, 142, 13550−13557

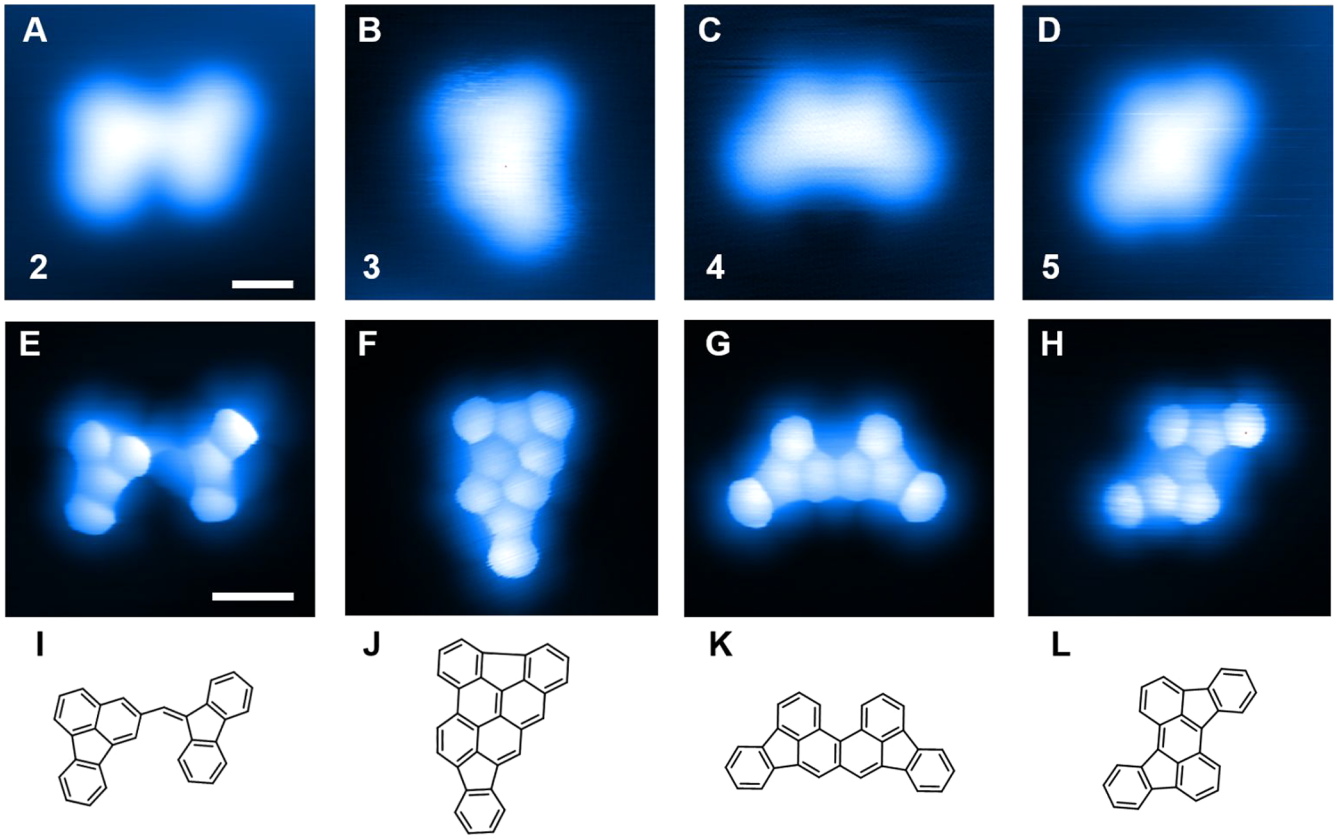

Figure 3. STM images of different products after thermally annealing of monoradical **1a** on Au(111). (A−D) Constant current STM images (CO tip, I = 100 pA, V = 1.5 V) of the products **2**, **3**, **4**, and **5**, respectively. Scale bar is 0.5 nm. (E−H) Bond-resolved STM images (CO tip, V = 50 mV) of the products corresponding to (A−D), respectively. Scale bar is 0.5 nm. (I−L) The identified molecular structures of four products corresponding to panels E−H, respectively.

spatial dependent dI/dV spectra. The delocalized spin density of the π-radical system of **1a** (Figure S2) not only leads to a high stability but also facilitates to retain its spin on Au(111), consistent with DFT calculations (Figure 2D). All of these observations confirm the formation of monoradical **1a** by the removal of the central H atom of precursor **1**.

In order to probe intrinsic chemical reactivity and stability of monoradical **1a**, we conducted a gentle thermal annealing of the sample at 470 K in UHV conditions. BRSTM was used to investigate the thermal induced structural dissociation and rearrangement of **1a** on Au(111). We managed to capture four products as shown in Figure 2F, namely, **2**, **3**, **4**, and **5** with a yield of 92.4%, 4.1%, 1.8%, and 1.7% respectively (Figure S3). The constant current STM images of these different products exhibit rather blur microscopic contrasts arising from the electronic local density of states (LDOS) associated with the molecular-orbitals (Figure 3A−D). By contrast, the constant height BRSTM images (Figure 3E−H) with CO-functionalized tip unambiguously reveal the backbone of molecule at the single atomic bond level, whereby the corresponding molecular structures can be identified (Figure 3I−L).[32,33]

Based on the structures resolved by BRSTM, we then proposed the possible reaction pathways toward the formation of these different products derived from monoradical **1a** on Au (111) (Figure 3). Generally, a cascade multiple-step reaction is required to form these different products, which involve (i) the structural dissociation of monoradical **1a** via breaking one of the C−C bonds of the central isobutane group to form two molecular fragments (fluorene radical and **2**); (ii) a homocoupling of the fluorene radical fragments followed by bond rearrangement results in the formation of product **5**; and (iii) the formation of product **3** and **4** through the multiple intramolecular dehydrogenation and cyclization of product **2**.

We then performed DFT calculations of reaction energetics of elementary steps to probe the feasibility of these proposed reaction pathways. Figure 4 shows the adsorption configurations and energies of various species on Au (111). The calculations reveal an adsorption energy of −0.32 eV for the monoradical molecule on Au(111) with a nearly flat geometry (**1a** in Figure 4A,B) rather than a highly tilted three-dimensional configuration in the gas phase. A possible cyclic intermediate (**1c** in Figure 4A,B) can be formed through the electrocyclization of monoradical (**1a**-**1b**, Figure 4A) with an uphill reaction energy of 1.11 eV. It is likely that the decomposition of the cyclic intermediate produces a **FR** and product **2** (**FR**+**2** in Figure 4A,B) with a downhill reaction energy of −1.18 eV.

Product **2** can be further transformed into products **3** and **4** via Scholl reactions as shown in Figure 5.[34−36] The fluorene and fluoranthene motifs of products **2** are connected by a joint single and double C−C bonds. A flip of these two motifs via the single C−C bond leads to the formation of a second conformation **2a**. However, the absence of **2a** in our experiment indicates that **2a** is energetically less favorable than **2**. Nevertheless, further thermal annealing may trigger the transition from **2** to **2a**. A subsequent C1−C6 cyclization of the fluorene and fluoranthene groups in **2** (**2a**) generates product **2b** (**4**), respectively (Figure 5), consistent with a

https://dx.doi.org/10.1021/jacs.0c05337
J. Am. Chem. Soc. 2020, 142, 13550−13557

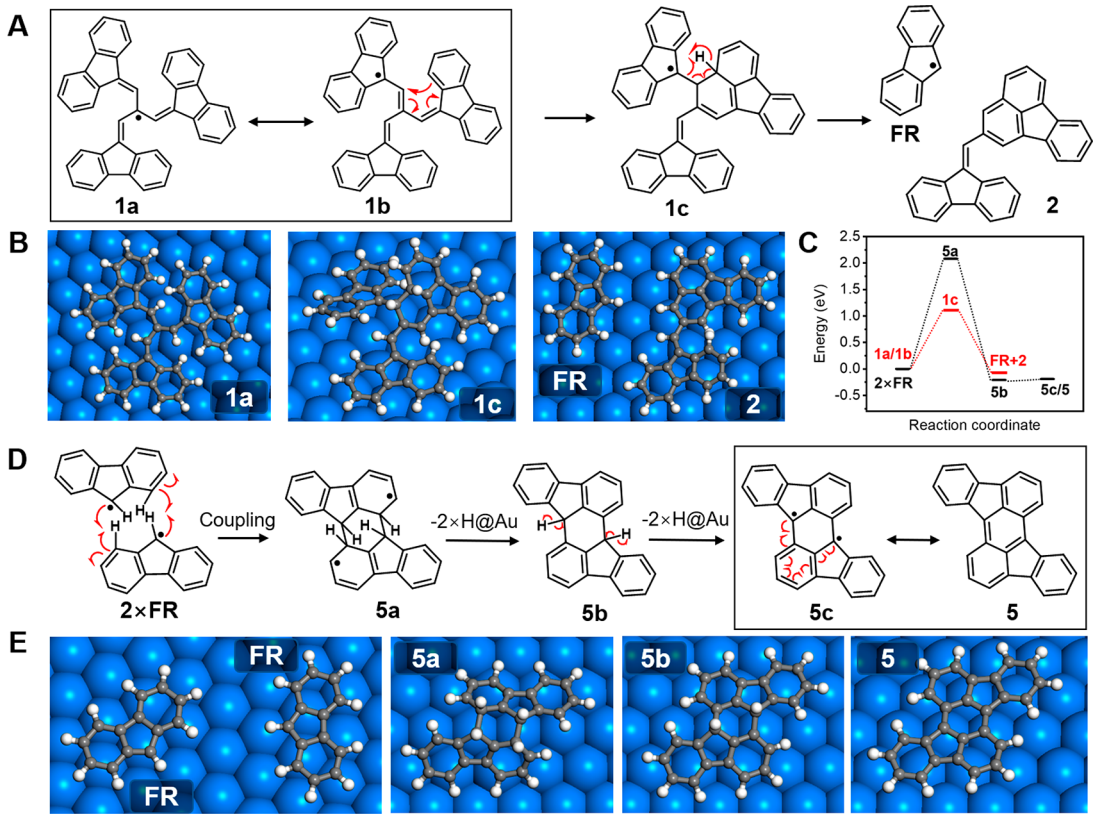

Figure 4. (A) Proposed reaction pathway for the dissociation and structural rearrangement of monoradical **1a** to form product **2** and fluorene radical (FR) on Au(111). (B) DFT-modeled structures of **1a**, **1c**, and **FR** + **2** on Au(111). (C) Energy diagrams of the proposed reaction pathways as shown in panels A and D. (D) Proposed reaction pathway for the coupling reaction of two fluorene radicals into rubicene **5**. (E) DFT-modeled structures of 2 × **FR**, **5a**, **5b**, and **5** on Au(111).

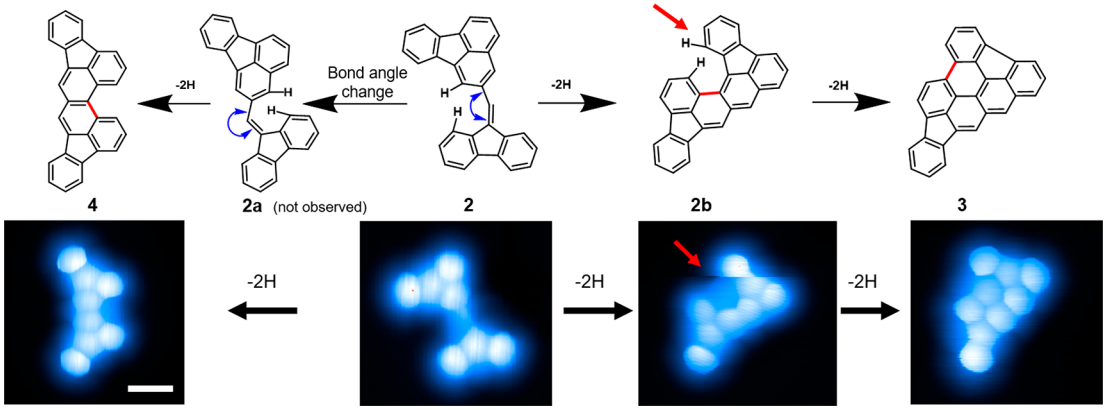

Figure 5. Proposed reaction pathways from product **2** to products **3** and **4** respectively. The corresponding BRSTM image of reaction intermediates and products are shown in the bottom panel (CO tip, V = 50 mV). The red C−C bonds in **2b**, **3**, and **4** indicate newly formed chemical bonds from the last step. The red arrow indicates the position of **2b** (up-tilted benzene ring as a result of steric hindrance) where the lateral movement occurs during scanning. Scale bars for all the STM images are 0.5 nm.

previous report that a similar cyclodehydrogenation can be triggered by light irradiation in tetrahydrofuran solution with iodine as a catalyst.[37] Similarly, a further cyclodehydrogenation of **2b** results in the formation of product **3**.

To our surprise, rubicene (product **5**) was also obtained as shown in Figure 3D,H. As a molecular fragment of C_{70}, rubicene has been proved as a promising organic semiconductor with excellent electronic characteristics for organic electronics. The formation of **5** was proposed to involve the coupling of two dissociated **FRs**. Thermal diffusion of these **FR** intermediates allows for the intermolecular coupling toward a cascade dimerization reaction to form **5** on Au(111) (Figure S4). A low yield of rubicene is probably attributed to two factors (i) a low probability of intermolecular coupling and (ii) the desorption of the small-sized fluorene radicals from Au(111) during thermal annealing. Our calculations also reveal that the coupling of two **FRs** (**5a** in Figure 4D,E) is required to overcome an energy barrier larger than 2.08 eV, to form the cyclized intermediate followed by the dehydrogenation via a removal of two H atoms, to produce an

https://dx.doi.org/10.1021/jacs.0c05337
J. Am. Chem. Soc. 2020, 142, 13550−13557

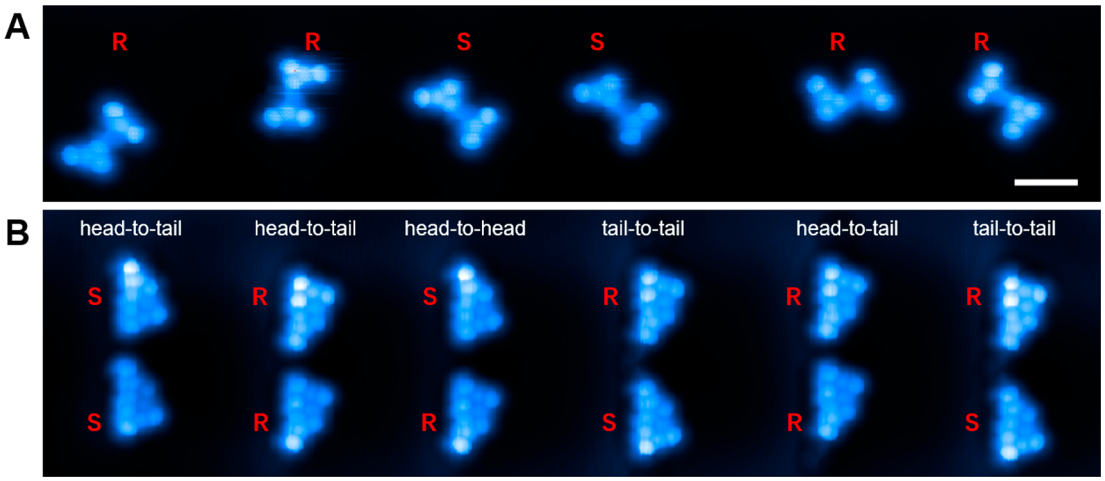

Figure 6. (A) BRSTM images of product **2** show a surface-induced chirality (CO tip, V = 50 mV). (B) BRSTM images reveal the pairing of product **3** enantiomer at the elbow sites with three different alignment configurations, head-to-tail, head-to-head, and tail-to-tail (CO tip, V = 50 mV). Scale bar 1 nm.

intermediate **5b**. The reaction energy for the first step dehydrogenation is determined to be −2.29 eV. A further dehydrogenation leads to the formation of rubicene with a reaction energy of 0.02 eV (**5** in Figure 4D,E). A common synthetic method of rubicene and its derivatives involves three consecutive steps including the conversion of commercial antraquinone into diol, followed by its reduction into dichloroanthracene and subsequent cyclization into rubicene.[38] Here, a facial synthetic strategy of rubicene can be achieved on Au(111), which may open up a new avenue for the synthesis of rubicene and its derivatives.

Surface-Absorption Induced Chirality. In addition to the real-space imaging of reaction products, the submolecular resolution capability of BRSTM also allows us to identify the chirality of reaction products imprinted onto the metal in large-scale imaging.[39,40] Interestingly, monoradical **1a** (Figure 2E, inset), product **2**, and product **3** (Figure 6A,B) are achiral in gas phase but show a surface-absorption induced chirality. The enantiomers of product **2** can transform from one to another through the flip of fluoranthene motif in the gas phase. However, this is not likely to occur on surface because of a high energy barrier arising from a large size of these molecular motifs. Therefore, the two enantiomers of product **2** are most likely to derive from their corresponding enantiomers of the reactant, monoradical **1a** (Figure 2E, inset).[41] Typically, the enantiomers of these products are randomly distributed over the surface. Notably, we observed that enantiomers of product **3** are often paired close to each other at the elbows of the herringbones (Figures S5 and 6B).[42,43] These enantiomer pairs adopt three different alignments at the elbow sites including head-to-head, head-to-tail, and tail-to-tail, which can be attributed to a strong chemical interaction for a pair of enantiomers in this region of space with a high chemical reactivity.

CONCLUSION

In summary, we have demonstrated the capability of BRSTM to probe the surface reaction of a monoradical at the single molecule level. BRSTM with submolecular resolution are exploited to directly visualize internal covalent bond configurations of various reaction intermediates and products derived from the dissociation and rearrangement of mono-radicals on the surface, which also shed light on the mysterious radical degradation process in solution phase. Real-space imaging of single-molecule reactions via BRSTM provides detailed mechanism insights into the complexed radical reactions on the surface, which in turn guides the design and synthesis of stable radical species toward material processing and quantum device fabrication.

ASSOCIATED CONTENT

Supporting Information

The Supporting Information is available free of charge at https://pubs.acs.org/doi/10.1021/jacs.0c05337.

Scheme S1, Figure S1−S7, methods and instruments, synthetic procedures for precursor **1**; computational details; and NMR spectra (PDF)

Crystallographic data for compound **2** (CIF)

Crystallographic data for compound **1** (CIF)

AUTHOR INFORMATION

Corresponding Author

Jiong Lu − *Department of Chemistry and Centre for Advanced 2D Materials (CA2DM), National University of Singapore, Singapore 117543 Singapore;* orcid.org/0000-0002-3690-8235; Email: chmluj@nus.edu.sg

Authors

Shaotang Song − *Department of Chemistry, National University of Singapore, Singapore 117543 Singapore; SZU-NUS Collaborative Center, International Collaborative Laboratory of 2D Materials for Optoelectronic Science & Technology of Ministry of Education, Engineering Technology Research Center for 2D Materials Information Functional Devices and Systems of Guangdong Province, Institute of Microscale Optoelectronics, Shenzhen University, Shen Zhen 518060, China;* orcid.org/0000-0003-3487-3566

Na Guo − *Department of Physics, National University of Singapore, Singapore 117542 Singapore*

Xinzhe Li − *Department of Chemistry, National University of Singapore, Singapore 117543 Singapore*

Guangwu Li − *Department of Chemistry, National University of Singapore, Singapore 117543 Singapore*

Yohei Haketa − *Department of Applied Chemistry, College of Life Sciences, Ritsumeikan University, Kusatsu 525-8577, Japan*
Mykola Telychko − *Department of Chemistry and Centre for Advanced 2D Materials (CA2DM), National University of Singapore, Singapore 117543 Singapore*
Jie Su − *Department of Chemistry and Centre for Advanced 2D Materials (CA2DM), National University of Singapore, Singapore 117543 Singapore*
Pin Lyu − *Department of Chemistry, National University of Singapore, Singapore 117543 Singapore*
Zhizhan Qiu − *Department of Chemistry, National University of Singapore, Singapore 117543 Singapore*
Hanyan Fang − *Department of Chemistry, National University of Singapore, Singapore 117543 Singapore*
Xinnan Peng − *Department of Chemistry, National University of Singapore, Singapore 117543 Singapore*
Jing Li − *Department of Chemistry, National University of Singapore, Singapore 117543 Singapore;* orcid.org/0000-0002-5627-4153
Xinbang Wu − *Department of Chemistry, National University of Singapore, Singapore 117543 Singapore*
Ying Li − *SZU-NUS Collaborative Center, International Collaborative Laboratory of 2D Materials for Optoelectronic Science & Technology of Ministry of Education, Engineering Technology Research Center for 2D Materials Information Functional Devices and Systems of Guangdong Province, Institute of Microscale Optoelectronics, Shenzhen University, Shen Zhen 518060, China*
Chenliang Su − *SZU-NUS Collaborative Center, International Collaborative Laboratory of 2D Materials for Optoelectronic Science & Technology of Ministry of Education, Engineering Technology Research Center for 2D Materials Information Functional Devices and Systems of Guangdong Province, Institute of Microscale Optoelectronics, Shenzhen University, Shen Zhen 518060, China;* orcid.org/0000-0002-8453-1938
Ming Joo Koh − *Department of Chemistry, National University of Singapore, Singapore 117543 Singapore;* orcid.org/0000-0002-2534-4921
Jishan Wu − *Department of Chemistry, National University of Singapore, Singapore 117543 Singapore;* orcid.org/0000-0002-8231-0437
Hiromitsu Maeda − *Department of Applied Chemistry, College of Life Sciences, Ritsumeikan University, Kusatsu 525-8577, Japan;* orcid.org/0000-0001-9928-1655
Chun Zhang − *Department of Chemistry, Department of Physics, and Centre for Advanced 2D Materials (CA2DM), National University of Singapore, Singapore 117543 Singapore;* orcid.org/0000-0002-1581-5806

Complete contact information is available at: https://pubs.acs.org/10.1021/jacs.0c05337

Author Contributions

[#]S.S. and N.G. contributed equally.

Notes

The authors declare no competing financial interest.

■ ACKNOWLEDGMENTS

J.L. acknowledges the support from MOE Grants (MOE2017-T2-1-056 and R-143-000-A75-114), NRF-CRP Grant (NRF-CRP16-2015-02), and NUS flagship green energy program (R-143-000-A55-646). C.Z. acknowledges the support from NUS academic research fund (R-144-000-410-114) and NUS green energy program (R-143-000-A63-114). Computational works were performed at the Graphene Research Centre computing cluster facilities. H.M. acknowledges the support from JSPS KAKENHI Grant Numbers JP26288042 and JP18H01968 for Scientific Research (B), JP26107007 for Scientific Research on Innovative Areas "Photosynergetics", and Ritsumeikan Global Innovation Research Organization (R-GIRO) project (2017-22). We thank Dr. Nobuhiro Yasuda, JASRI, and Prof. Hikaru Takaya, Kyoto University, for synchrotron radiation single-crystal analyses (SPring-8:2018A1173) and Prof. Ichiro Hisaki, Osaka University, for synchrotron radiation single-crystal analyses (SPring-8:2018A1327).

■ REFERENCES

(1) Gomberg, M. An instance of trivalent carbon: triphenylmethyl. *J. Am. Chem. Soc.* **1900**, *22*, 757.
(2) Ratera, I.; Veciana, J. Playing with organic radicals as building blocks for functional molecular materials. *Chem. Soc. Rev.* **2012**, *41* (1), 303−349.
(3) Frisenda, R.; Gaudenzi, R.; Franco, C.; Mas-Torrent, M.; Rovira, C.; Veciana, J.; Alcon, I.; Bromley, S. T.; Burzurí, E.; Van der Zant, H. S. Kondo effect in a neutral and stable all organic radical single molecule break junction. *Nano Lett.* **2015**, *15*, 3109−3114.
(4) Gallagher, N. M.; Olankitwanit, A.; Rajca, A. High-spin organic molecules. *J. Org. Chem.* **2015**, *80*, 1291−1298.
(5) Liu, J.; Isshiki, H.; Katoh, K.; Morita, T.; Breedlove, B. K.; Yamashita, M.; Komeda, T. First observation of a Kondo resonance for a stable neutral pure organic radical, 1,3,5-triphenyl-6-oxoverdazyl, adsorbed on the Au (111) surface. *J. Am. Chem. Soc.* **2013**, *135*, 651−658.
(6) Wang, X.-Y.; Avendaño, C.; Dunbar, K. R. Molecular magnetic materials based on 4d and 5d transition metals. *Chem. Soc. Rev.* **2011**, *40*, 3213−3238.
(7) Liu, C.; Ni, Y.; Lu, X.; Li, G.; Wu, J. Global aromaticity in macrocyclic polyradicaloids: Hückel's Rule or Baird's Rule? *Acc. Chem. Res.* **2019**, *52*, 2309−2321.
(8) Tian, Y.; Uchida, K.; Kurata, H.; Hirao, Y.; Nishiuchi, T.; Kubo, T. Design and synthesis of new stable fluorenyl-based radicals. *J. Am. Chem. Soc.* **2014**, *136*, 12784−12793.
(9) Riss, A.; Paz, A. P.; Wickenburg, S.; Tsai, H.-Z.; De Oteyza, D. G.; Bradley, A. J.; Ugeda, M. M.; Gorman, P.; Jung, H. S.; Crommie, M. F.; Rubio, A.; Fischer, F. R. Imaging single-molecule reaction intermediates stabilized by surface dissipation and entropy. *Nat. Chem.* **2016**, *8*, 678−683.
(10) de Oteyza, D. G.; Gorman, P.; Chen, Y.-C.; Wickenburg, S.; Riss, A.; Mowbray, D. J.; Etkin, G.; Pedramrazi, Z.; Tsai, H.-Z.; Rubio, A.; Crommie, M. F.; Fischer, F. R. Direct imaging of covalent bond structure in single-molecule chemical reactions. *Science* **2013**, *340*, 1434−1437.
(11) Jiang, Y.; Huan, Q.; Fabris, L.; Bazan, G. C.; Ho, W. Submolecular control, spectroscopy and imaging of bond-selective chemistry in single functionalized molecules. *Nat. Chem.* **2013**, *5*, 36−41.
(12) Nguyen, G. D.; Tsai, H.-Z.; Omrani, A. A.; Marangoni, T.; Wu, M.; Rizzo, D. J.; Rodgers, G. F.; Cloke, R. R.; Durr, R. A.; Sakai, Y.; Liou, F.; Aikawa, A. S.; Chelikowsky, J. R.; Louie, S. G.; Fischer, F. R.; Crommie, M. F. Atomically precise graphene nanoribbon heterojunctions from a single molecular precursor. *Nat. Nanotechnol.* **2017**, *12*, 1077−1082.
(13) Hapala, P.; Kichin, G.; Wagner, C.; Tautz, F. S.; Temirov, R.; Jelínek, P. Mechanism of high-resolution STM/AFM imaging with functionalized tips. *Phys. Rev. B: Condens. Matter Mater. Phys.* **2014**, *90*, 085421.
(14) Gross, L.; Mohn, F.; Moll, N.; Liljeroth, P.; Meyer, G. The chemical structure of a molecule resolved by atomic force microscopy. *Science* **2009**, *325*, 1110−1114.

(15) Su, J.; Telychko, M.; Hu, P.; Macam, G.; Mutombo, P.; Zhang, H.; Bao, Y.; Cheng, F.; Huang, Z.-Q.; Qiu, Z.; Tan, S. J. R.; Lin, H.; Jelinek, P.; Chuang, F.-C.; Wu, J.; Lu, J. Atomically precise bottom-up synthesis of π-extended [5] triangulene. *Sci. Adv.* **2019**, *5*, No. eaav7717.
(16) Schuler, B.; Fatayer, S.; Mohn, F.; Moll, N.; Pavliček, N.; Meyer, G.; Peña, D.; Gross, L. Reversible Bergman cyclization by atomic manipulation. *Nat. Chem.* **2016**, *8*, 220−224.
(17) Pavliček, N.; Gawel, P.; Kohn, D. R.; Majzik, Z.; Xiong, Y.; Meyer, G.; Anderson, H. L.; Gross, L. Polyyne formation *via* skeletal rearrangement induced by atomic manipulation. *Nat. Chem.* **2018**, *10*, 853−858.
(18) Li, J.; Sanz, S.; Corso, M.; Choi, D. J.; Peña, D.; Frederiksen, T.; Pascual, J. I. Single spin localization and manipulation in graphene open-shell nanostructures. *Nat. Commun.* **2019**, *10*, 1−7.
(19) Mishra, S.; Beyer, D.; Eimre, K.; Ortiz, R.; Fernandez-Rossier, J.; Berger, R.; Groning, O.; Pignedoli, C. A.; Fasel, R.; Feng, X.; Ruffieux, P. Collective all-carbon magnetism in triangulene dimers. *Angew. Chem., Int. Ed.* **2020**, *59*, 12041−12047.
(20) Mishra, S.; Beyer, D.; Berger, R.; Liu, J.; Groening, O.; Urgel, J. I.; Müllen, K.; Ruffieux, P.; Feng, X.; Fasel, R. Topological defect-induced magnetism in a nanographene. *J. Am. Chem. Soc.* **2020**, *142*, 1147−1152.
(21) Gross, L. Recent advances in submolecular resolution with scanning probe microscopy. *Nat. Chem.* **2011**, *3*, 273−278.
(22) Kawai, S.; Takahashi, K.; Ito, S.; Pawlak, R.; Meier, T.; Spijker, P.; Canova, F. F.; Tracey, J.; Nozaki, K.; Foster, A. S.; Meyer, E. Competing annulene and radialene structures in a single anti-aromatic molecule studied by high-resolution atomic force microscopy. *ACS Nano* **2017**, *11*, 8122−8130.
(23) de Oteyza, D. G.; Perez Paz, A.; Chen, Y.-C.; Pedramrazi, Z.; Riss, A.; Wickenburg, S.; Tsai, H.-Z.; Fischer, F. R.; Crommie, M. F.; Rubio, A. Noncovalent dimerization after enediyne cyclization on Au (111). *J. Am. Chem. Soc.* **2016**, *138*, 10963−10967.
(24) Fittig, R.; Ostermayer, E. Ueber das Phenanthren, einen neuen Kohlenwasserstoff im Steinkohlentheer. *Justus Liebigs Annalen der Chemie* **1873**, *166*, 361−382.
(25) Okamoto, K.; Kitagawa, T.; Takeuchi, K.; Komatsu, K.; Kinoshita, T.; Aonuma, S.; Nagai, M.; Miyabo, A. Isolation and properties of hydrocarbon salts. *J. Org. Chem.* **1990**, *55*, 996−1002.
(26) Frota, H. Shape of the Kondo resonance. *Phys. Rev. B: Condens. Matter Mater. Phys.* **1992**, *45*, 1096.
(27) Ternes, M. Spin excitations and correlations in scanning tunneling spectroscopy. *New J. Phys.* **2015**, *17*, 063016.
(28) Újsághy, O.; Kroha, J.; Szunyogh, L.; Zawadowski, A. Theory of the Fano resonance in the STM tunneling density of states due to a single Kondo impurity. *Phys. Rev. Lett.* **2000**, *85*, 2557.
(29) Patera, L. L.; Sokolov, S.; Low, J. Z.; Campos, L. M.; Venkataraman, L.; Repp, J. Resolving the unpaired-electron orbital distribution in a stable organic radical by kondo resonance mapping. *Angew. Chem., Int. Ed.* **2019**, *58*, 11063−11067.
(30) Mishra, S.; Beyer, D.; Eimre, K.; Kezilebieke, S.; Berger, R.; Groning, O.; Pignedoli, C. A.; Mullen, K.; Liljeroth, P.; Ruffieux, P.; Feng, X.; Fasel, R. Topological frustration induces unconventional magnetism in a nanographene. *Nat. Nanotechnol.* **2020**, *15*, 22−28.
(31) Zhang, Y.-H.; Kahle, S.; Herden, T.; Stroh, C.; Mayor, M.; Schlickum, U.; Ternes, M.; Wahl, P.; Kern, K. Temperature and magnetic field dependence of a Kondo system in the weak coupling regime. *Nat. Commun.* **2013**, *4*, 1−6.
(32) Kichin, G.; Wagner, C.; Tautz, F.; Temirov, R. Calibrating atomic-scale force sensors installed at the tip apex of a scanning tunneling microscope. *Phys. Rev. B: Condens. Matter Mater. Phys.* **2013**, *87*, 081408.
(33) Zhang, J.; Chen, P.; Yuan, B.; Ji, W.; Cheng, Z.; Qiu, X. Real-space identification of intermolecular bonding with atomic force microscopy. *Science* **2013**, *342*, 611−614.
(34) Treier, M.; Pignedoli, C. A.; Laino, T.; Rieger, R.; Müllen, K.; Passerone, D.; Fasel, R. Surface-assisted cyclodehydrogenation provides a synthetic route towards easily processable and chemically tailored nanographenes. *Nat. Chem.* **2011**, *3*, 61−67.
(35) Rempala, P.; Kroulík, J.; King, B. T. Investigation of the mechanism of the intramolecular Scholl reaction of contiguous phenylbenzenes. *J. Org. Chem.* **2006**, *71*, 5067−5081.
(36) Rempala, P.; Kroulík, J.; King, B. T. A slippery slope: mechanistic analysis of the intramolecular Scholl reaction of hexaphenylbenzene. *J. Am. Chem. Soc.* **2004**, *126*, 15002−15003.
(37) Jutz, C.; Lobering, H.-G. A Novel Simple Synthesis of Helicenes. *Angew. Chem., Int. Ed. Engl.* **1975**, *14*, 418−420.
(38) Smet, M.; Shukla, R.; Fulop, L.; Dehaen, W. A general synthesis of disubstituted rubicenes. *Eur. J. Org. Chem.* **1998**, *1998*, 2769−2773.
(39) Park, J.; Kim, J. H.; Bak, S.; Tahara, K.; Jung, J.; Kawai, M.; Tobe, Y.; Kim, Y. On-Surface evolution of meso-isomerism in two-dimensional supramolecular assemblies. *Angew. Chem., Int. Ed.* **2019**, *58*, 9611−9618.
(40) Sakaguchi, H.; Song, S.; Kojima, T.; Nakae, T. Homochiral polymerization-driven selective growth of graphene nanoribbons. *Nat. Chem.* **2017**, *9*, 57−63.
(41) Merino-Diez, N.; Mohammed, M. S. G.; Castro-Esteban, J.; Colazzo, L.; Berdonces-Layunta, A.; Lawrence, J.; Pascual, J. I.; de Oteyza, D. G.; Pena, D. Transferring Axial Molecular Chirality Through a Sequence of On-Surface Reactions. *Chem. Sci.* **2020**, *11*, 5441−5446.
(42) Böhringer, M.; Morgenstern, K.; Schneider, W.; Berndt, R. Two-dimensional self-assembly of magic supramolecular clusters. *J. Phys.: Condens. Matter* **1999**, *11*, 9871.
(43) Kumagai, T.; Ladenthin, J. N.; Litman, Y.; Rossi, M.; Grill, L.; Gawinkowski, S.; Waluk, J.; Persson, M. Quantum tunneling in real space: Tautomerization of single porphycene molecules on the (111) surface of Cu, Ag, and Au. *J. Chem. Phys.* **2018**, *148*, 102330.

https://dx.doi.org/10.1021/jacs.0c05337
J. Am. Chem. Soc. 2020, 142, 13550−13557